


CO₂ hydrogenation to methanol on tungsten-doped Cu/CeO₂ catalysts

Journal Article

Author(s):

Yan, Yong; Wong, Roong Jien; Ma, Zhirui; [Donat, Felix](#) ; Xi, Shibo; Saqline, Syed; Fan, Qianwenhao; Du, Yonghua; Borgna, Armando; He, Qian; Müller, Christoph R.; Chen, Wei; Lapkin, Alexei A.; Liu, Wen

Publication date:

2022-06-05

Permanent link:

<https://doi.org/10.3929/ethz-b-000532673>

Rights / license:

[Creative Commons Attribution-NonCommercial-NoDerivatives 4.0 International](#)

Originally published in:

Applied Catalysis B: Environmental 306, <https://doi.org/10.1016/j.apcatb.2022.121098>

CO₂ Hydrogenation to Methanol on Tungsten-Doped Cu/CeO₂ Catalysts

Yong Yan,^{[a],[b]} Roong Jien Wong,^{[a][b][c]} Zhirui Ma,^[d] Felix Donat,^[e] Shibo Xi,^[f] Syed Saqline,^{[a],[b],[c]} Qianwenhao Fan,^{[a][b]} Yonghua Du,^{[f],[g]} Armando Borgna,^[f] Qian He,^[h] Christoph R. Müller,^[e] Wei Chen,^[d] Alexei A. Lapkin,^{[b],[i]} Wen Liu*^{[a],[b]}

[a] School of Chemical and Biomedical Engineering, Nanyang Technological University, 62 Nanyang Drive, Singapore 637459, Singapore

[b] Cambridge Centre for Advanced Research and Education, 1 Create Way, #05-05 Singapore 138602, Singapore

[c] Nanyang Environmental and Water Research Institute, Nanyang Technological University, 1 Cleantech Loop, Singapore 637141, Singapore

[d] Department of Chemistry, National University Singapore, 3 Science Drive 3, Singapore 117543, Singapore

[e] Department of Mechanical and Process Engineering, ETH Zurich, Leonhardstrasse 21 8092 Zürich, Switzerland

[f] Institute of Chemical and Engineering Sciences, Agency for Science, Technology and Research, 1 Pesek Road, Singapore 627833, Singapore

[g] Brookhaven National Laboratory, National Synchrotron Light Source II, Bldg. 743, P.O. Box 5000, Upton, NY 11973-500, United States

[h] Department of Materials Science and Engineering, National University Singapore, 9 Engineering Drive 1, Singapore 117575, Singapore

[i] Department of Chemical Engineering and Biotechnology, University of Cambridge, Philippa Fawcett Drive, Cambridge, CB3 0AS, United Kingdom

KEYWORDS: CO₂, methanol, oxygen vacancy, hydrogenation, ceria, metal-support interface

ABSTRACT

The catalytic hydrogenation of CO₂ to methanol depends significantly on the structures of metal-oxide interfaces. We show that doping a high-valency metal, viz. tungsten, to CeO₂ could render improved catalytic activity for the hydrogenation of CO₂ on a Cu/CeW_{0.25}O_x catalyst, whilst making it more selective towards methanol than the undoped Cu/CeO₂. We experimentally investigated and elucidated the structural-functional relationship of the Cu/CeO₂ interface for CO₂ hydrogenation. The promotional effects are attributed to the irreversible reduction of Ce⁴⁺ to Ce³⁺ by W-doping, the suppression of the formation of redox-active oxygen vacancies on CeO₂, and the activation of the formate pathway for CO₂ hydrogenation. This catalyst design strategy differs fundamentally from those commonly used for CeO₂-supported catalysts, in which oxygen vacancies with high redox activity are considered desirable.

1. INTRODUCTION

Carbon capture, storage and utilisation (CCSU) is a scheme that complements the transition to renewable energies and electrification towards building a low-carbon economy.¹⁻⁴ An important aspect of CCSU is to synthesize, at large scale, chemicals and fuels from captured CO₂.^{5,6} Amongst the various CO₂-derived products, methanol is a highly attractive target, owing to its versatile roles as a gateway molecule and a liquid fuel substitute.⁷⁻¹⁰ Recent analyses have shown that methanol synthesised from captured CO₂ and renewable hydrogen has a significantly lower environmental impact than that produced from natural gas or coal.¹¹ Furthermore, the use of methanol as a fuel additive could substantially reduce CO₂ emission from vehicle exhaust.¹²

To date, there is limited commercial processes that produces methanol from CO₂,^{13,14} partly because the commercial Cu/ZnO/Al₂O₃ methanol synthesis catalysts are insufficiently stable under the CO₂ hydrogenation conditions.^{15,16} Meanwhile, several catalysts with promising performance have been developed and evaluated at pilot scales.¹⁷⁻²³ Significant experimental and theoretical research have been conducted to establish reaction pathways of methanol synthesis. It is generally understood that the activation of CO₂ is the first rate-limiting step. Depending on the nature of the active sites, CO₂ may form formate (HCOO*), carboxyl (*COOH), carbonate (*CO₃), bicarbonate (*HCO₃), or a surface carbonyl (*CO) upon adsorption.^{24,25} The further hydrogenation of the surface intermediates; e.g. HCOO* and *CO, is regarded as the second rate-limiting step.^{25,26} This is followed by the successive hydrogenation to form *CH₃O, the hydrogenation and desorption of which is the final step to methanol production. According to the second rate-limiting step, the reaction mechanisms are classified as (i) the formate pathway, where HCOO* is a key reaction intermediate, or (ii) the reverse water-gas-shift (RWGS) pathway, where *COOH or *CO are key reaction intermediates.²⁵ However, the identities of the active sites of many high-performing catalysts remain debatable and the structural-functional relationships at the metal-oxide interfaces

are yet to be fully understood.^{13,16,27–29} For any metal/oxide interface catalysts, closing these knowledge gaps will enable the rapid improvement of catalyst design.

Amongst the various Cu-based catalysts, Cu/CeO₂ is known to catalyse methanol synthesis via the RWGS pathway, where CO is produced as a reaction intermediate as well as a byproduct. However, unmodified Cu/CeO₂ shows relatively low activity (space time yield, STY < 2 mol_{MeOH}·kg_{cat}⁻¹·h⁻¹) and moderate selectivity (~50%).^{30,31} Attempts to improve the activities of CeO₂-based catalysts often evolve around promoting their redox activity, e.g. by preparing morphologically well-defined CeO₂ supports with high redox activities^{32,33} or doping lower-valency cations (e.g. Co³⁺ and Pr³⁺) to generate additional oxygen vacancies.^{34–38} These approaches invariably promote RWGS and the formation of CO, whose adsorption on Cu is weak, therefore limiting the overall methanol productivity and selectivity.^{39–41}

According to recent studies,^{35,42} doping high-valency metals such as Mo and W will reduce CeO₂ as the dopants donate electrons to adjacent Ce⁴⁺. Such reduction does not involve the generation of additional oxygen vacancies and is therefore fundamentally different from the conventional reduction by lattice oxygen removal. Therefore, this doping effect offers an alternative approach to modify the activity of Cu/CeO₂ without generating additional oxygen vacancies.⁴³ Here, we successfully prepared a W-doped Cu/CeO₂ catalyst, viz. Cu/CeW_{0.25}O_x, which shows a substantially enhanced methanol activity (CO₂ conversion = 13%, STY = 12.32 mol_{MeOH}·kg_{cat}⁻¹·h⁻¹) over unmodified Cu/CeO₂ (CO₂ conversion = 1.3%, STY = 1.26 mol_{MeOH}·kg_{cat}⁻¹·h⁻¹) at 250 °C, 35 bar total pressure and a weight hourly space velocity (WHSV) of 15000 mL g_{cat}⁻¹ h⁻¹. The Cu/CeW_{0.25}O_x catalyst is also significantly more selective towards methanol (87% vs. 51%) than the undoped Cu/CeO₂. In fact, the activity of Cu/CeW_{0.25}O_x is on par with some of the best performing Cu-based CO₂-to-methanol catalysts reported in the literature.^{44–51} In situ vibrational

spectroscopy and *in situ* X-ray scattering experiments were conducted to elucidate the roles of different types of Ce^{3+} sites and oxygen vacancies during methanol synthesis.

2. EXPERIMENTAL

2.1. Catalyst preparation

All chemicals were purchased from Sigma Aldrich and used as received without further purification. To prepare W-doped CeO_2 , urea was added into an aqueous $\text{Ce}(\text{NO}_3)_3$ solution (0.005 M) at a urea : Ce^{3+} ratio of 10 : 1. Then, $(\text{NH}_4)_6\text{H}_2\text{W}_{12}\text{O}_{40}\cdot x\text{H}_2\text{O}$ (at a W : Ce ratio of 1 : 4), together with equal mass of $\text{H}_2\text{C}_2\text{O}_4\cdot 2\text{H}_2\text{O}$, was dissolved in the same solution. Subsequently, the solution was transferred into an autoclave, which was sealed and heated to 150 °C to react for 12 h. The resulting precipitate was filtered and washed with deionized water, dried at 100 °C overnight, and calcined at 500 °C for 1 h in air. Undoped CeO_2 was prepared by a similar procedure, but without $(\text{NH}_4)_6\text{H}_2\text{W}_{12}\text{O}_{40}\cdot x\text{H}_2\text{O}$ and $\text{H}_2\text{C}_2\text{O}_4\cdot 2\text{H}_2\text{O}$.

Supported Cu catalysts were prepared by wet impregnation. In a typical preparation, the support material (CeO_2 or W-doped CeO_2) was added to an aqueous solution containing required amount of $\text{Cu}(\text{NO}_3)_2$ under rigorous stirring. The targeted Cu loading was 10 wt%. After impregnation, the excess water was removed in a rotary evaporator at 80 °C. The catalysts were obtained by drying the resulting solid at 80 °C in air for 12 h, followed by calcination at 500 °C in air for 2 h.

2.2. Ex situ sample characterization

The crystalline structural information was investigated by powder X-ray diffraction (XRD) on a Bruker AXS D8 diffractometer with Cu $K\alpha$ radiation ($\lambda = 1.5406 \text{ \AA}$) at 40 kV and 40 mA. The morphology of the catalysts was examined by high-resolution transmission electron microscopy (HRTEM) using a JEOL JEM 2100F TEM, working at an accelerating voltage of 200 kV. The N_2 adsorption-desorption isotherms were measured on a Micromeritics 3 flex instrument at -196 °C.

Prior to N₂ physisorption, all samples were degassed at 180 °C for 5 h in vacuum. The specific surface areas were calculated according to the Brunauer-Emmet-Teller (BET) equation using the data over the P/P_0 range from 0.05 to 0.35. The X-ray photoelectron spectra (XPS) of the catalysts were acquired on a Kratos Axis Supra spectrophotometer with a dual anode monochromatic K α excitation source. All binding energies were calibrated against the adventitious carbon C 1s peak at 284.8 eV. Cu speciation was determined from the Auger electron spectroscopy with XPS.^{52,53}

Inductively coupled plasma optical emission spectroscopy (ICP-OES, Agilent 5100 VDV) was used to quantify the mass fractions of Cu, Ce, and W elements in the catalysts.

H₂ temperature-programmed reduction (H₂-TPR) measurements were carried out on a Micromeritics Autochem II 2920 instrument. Firstly, the catalysts were loaded into a quartz U-tube reactor and pretreated under an air flow (50 mL min⁻¹) at 500 °C for 60 min, followed by cooling to 35 °C in He. After 30 min, 5% H₂/N₂ (50 mL min⁻¹) was passed through the catalyst bed until a stable thermal conductivity detector (TCD) signal was observed. Subsequently, the temperature was increased from 35 °C to 1000 °C at a constant rate of 10 °C min⁻¹ in 5% H₂/N₂. The outlet gas, after H₂O removal, was analyzed by the TCD to quantify the consumption of H₂ during the TPR.

CO₂ temperature-programmed desorption (CO₂-TPD) was performed on the same Autochem II 2920 instrument equipped with a MKS Cirrus II mass spectrometer (MS). The total gas flow rate through the catalyst bed was kept constant at 50 mL/min. Prior to each TPD experiment, the sample (~100 mg) was pretreated in 5% H₂/N₂ at 500 °C for 60 min and cooled to 35 °C in He. At 35 °C, the sample was exposed to 10% CO₂/He for 60 min, followed by He purging for 30 min. Then, the temperature was raised to 500 °C at a ramping rate of 10 °C min⁻¹, whilst the mass spectrometer analysed the outlet gas and recorded the signals of CO ($m/z = 28$) and CO₂ ($m/z = 44$).

The surface dispersion of Cu metals was quantified by N₂O chemisorption measurements on a Micromeritics Autochem II 2920 instrument. In a typical measurement, Cu was first reduced in 10% H₂/Ar prior to N₂O chemisorption, followed by a second H₂ reduction step to remove the chemisorbed oxygen. H₂ reduction was first performed at 300 °C for 60 min. After cooling to room temperature, 10% N₂O/He was introduced to the sample until N₂O consumption was no longer observed. Hydrogen reduction, following the H₂-TPR program described above, was then conducted to quantify the amount of surface Cu atom based on the amount of H₂ consumed.

2.3. CO₂ hydrogenation to methanol

The performance of the catalyst was examined in a fixed-bed reactor. Before CO₂ hydrogenation, the loaded catalysts were reduced in situ in 50 mL min⁻¹ of 10% H₂/He at 500 °C and 10 bar for 60 min. In each experiment, 200 mg of catalyst was used to convert a 23:69:8 mixture of CO₂, H₂ and N₂, with a total flow rate of 50 mL min⁻¹ (STP) at 250 °C and 35 bar total pressure. Using N₂ as an internal standard, the composition of outlet gas was analyzed by online gas chromatography (Agilent 7890B) equipped with both flame ionization detector (FID) detector and TCD detector. Condensation of the liquid products was avoided by trace heating the gas sampling line to 90 °C. Kinetics data were collected by measuring the rate when the CO₂ conversion was below 10%.

2.4. In situ catalyst characterization

In situ diffuse reflectance infrared Fourier transform spectroscopy (DRIFTS) was carried out on a Bruker Tensor II FTIR spectrometer. The FTIR was equipped with a liquid-N₂ cooled MCT/A detector, a Pike DiffuseIR accessory, and a high-pressure reaction cell. Prior to each experiment, the sample was reduced in 50 mL min⁻¹ of 10% H₂/He at 500 °C for 60 min and cooled in He to the desired reaction temperature (250 °C). The background spectrum was collected in He, at the

reaction temperature. Each spectrum was obtained by averaging over 100 consecutive scans, each with a spectral resolution of 4 cm^{-1} .

In situ X-ray absorption spectra (XAS) were measured using wafer samples (I.D. 10 mm pellets) in a customized high pressure reaction cell equipped with two beryllium windows at the XAFCA beamline of Singapore Synchrotron Light Source (SSLS). The beamline has a flux of 1.6×10^{10} photons per second at 7 keV. A Si(111) crystal was used as the monochromator for the energy range from 2.1 to 12.8 keV. The typical scan time was about 20 min. The data were processed using IFEFFIT software packages. XAS of the as-prepared samples were measured at RT under He purging. The spectra of the reduced samples were collected after reduction in 10% H_2/He at 500 °C, 10 bar total pressure, for 60 min. In situ measurements were carried out when the samples were exposed to a 3:1 mixture of H_2 and CO_2 at 250 °C and 10 bar.

Near ambient pressure X-ray photoelectron spectroscopy (NAP-XPS) experiments were performed in a multichambered Specs system equipped with an Al/Mg twin anode X-ray source and a Phoibos hemispherical energy analyzer. A residual gas analyzer (RGA) was connected to the NAP lens chamber, which was exposed to 0.1 – 1 mbar of reaction gas, supplied through a 300 μm nozzle. The NAP cell was degassed before each experiment by heating to 627 °C under vacuum until the chamber pressure fell below 1×10^{-9} mbar. In each NAP-XPS experiment, the catalyst was first reduced in 0.4 mbar H_2 at 500 °C, followed by oxidation in 0.5 mbar CO_2 at RT. Then, 0.3 mbar CO_2 and 0.9 mbar H_2 were fed into the measurement chamber at 250 °C to simulate a CO_2 hydrogenation environment. Finally, the samples were oxidised in 0.4 mbar O_2 at 500 °C. NAP-XPS spectra were collected at each segment of the experiment, when the samples were believed to have reached steady state.

3. RESULTS AND DISCUSSION

3.1. Characterization of the as-prepared catalysts

[Figure 1](#) presents the characterisation of the as-synthesised CeO₂ supports and the Cu/CeO₂ catalysts, with and without W-doping. Prior to Cu loading, the X-ray diffraction (XRD) patterns of both the unmodified and the W-doped CeO₂ can be fully indexed by the fluorite-structured CeO₂ phase ([Figure S1](#)). After Cu loading, the freshly calcined catalysts show diffraction peaks of CuO, which changed to Cu after H₂ reduction ([Figures 1a](#)). In all cases, the absence of any diffraction peak associated with WO_x species suggests that W atoms are finely dispersed on and, or in the CeO₂ support. In addition, the samples containing W-doped CeO₂ show greater extent of peak broadening than the samples without W. This additional peak broadening effect is attributed to the additional microstrain (e.g. the presence of defects) that is commonly observed in metal-doped CeO₂.^{54–58} The lattice parameters of CeO₂ in the oxidized Cu/CeO₂ and Cu/CeW_{0.25}O_x catalysts were estimated by Rietveld refinement of the diffraction patterns to be 5.41 ± 0.01 and 5.44 ± 0.01 Å, respectively. The increase in the lattice parameter of CeO₂ upon W-doping signifies the reduction of Ce⁴⁺ to Ce³⁺.⁵⁹ In fact, both the reduced and oxidised forms of Cu/CeW_{0.25}O_x show larger CeO₂ lattices than the Cu/CeO₂ sample, suggesting the reduction of Ce⁴⁺ to Ce³⁺ by W doping is ubiquitous in all the chemical environments of interest. The HRTEM images, depicted in [Figures 1b](#) and [1c](#), show that both catalysts consist of grains of Cu and CeO₂ of ~ 4 nm and ~5 nm in size, respectively. The HRTEM observations further support the conclusion that the additional peak broadening of the W-doped CeO₂ observed in [Figure 1a](#) is due to increased microstrain rather than decreased grain sizes of CeO₂. The lattice fringes of 0.18 nm and 0.31 nm observed in the HRTEM images correspond to the Cu(200) and CeO₂(111) planes, respectively. Supplementary HRTEM images, including lower magnification ones, are provided in [Figure S2](#) of Supporting Information. The identification of the CeO₂ grains were further confirmed by selected

area electron diffraction (SAED) analysis, as shown [Figures S2c](#) and [S2d](#). It should be noted that the resolution of the present HRTEM analysis is not sufficiently high to verify the lattice expansion due to W-doping (as suggested by the XRD results). The actual Cu loadings on Cu/CeO₂ and Cu/CeW_{0.25}O_x, as determined by ICP-OES ([Table S1](#)), are 9.8 wt% and 10.9 wt%, respectively. The specific surface areas of the Cu/CeO₂ and Cu/CeW_{0.25}O_x catalysts, as determined by the BET analysis of the N₂ adsorption-desorption isotherms, are 105 and 84 m²g⁻¹, respectively. Given the lack of contrast of Cu on CeO₂ in TEM, the dispersion of Cu on the Cu/CeO₂ and Cu/CeW_{0.25}O_x catalysts is estimated by N₂O chemisorption (results shown in [Figure S3](#)), to be around 16.8 % and 16.9 %, respectively. Care is taken to discriminate the chemisorption signals associated with Cu and CeO₂. These dispersion values translate to mean Cu particle sizes of ~4.3 nm, assuming uniform particle sizes and spherical particle shape. The estimated particle sizes agree with the HRTEM ([Figure 1b](#) and [1c](#)), which show Cu particles of 4-5 nm in size. Therefore, despite the marginal increase in Cu loading and decrease in BET surface area, W-doping appears to have negligible effect on the morphology and dispersion of the supported Cu particles.

The chemical states of the surface regions of the catalysts were probed by XPS. The Ce 3d XPS spectra, shown in [Figure 1d](#), reflect the ratio of Ce³⁺ to Ce⁴⁺ in the surface region of the catalysts. On Cu/CeO₂, the major XPS peaks are assigned to a doublet of Ce⁴⁺ with an orbital splitting of ~18.6 eV, accompanied by the shakedown features of one or two electron transfer from a filled O 2p orbital to an empty Ce 4f orbital.⁶⁰ The doublet corresponding to Ce³⁺ is significantly more intense in the spectra of the Cu/CeW_{0.25}O_x than that of Cu/CeO₂, indicating that the reduction of Ce⁴⁺ by W was not only a bulk phenomenon, but also profound near the surface. The consequence of W-doping on the states of Cu at the Cu/oxide interfaces is analysed by Cu AES, as shown in [Figure S4a](#). Looking at the quantitative analyses of the fitted Cu Auger peaks, as shown in [Figure](#)

S4b, W-doping does not cause any significant change to the amount of Cu^+ in the surface region, where Cu^+ is regarded as the Cu species at the Cu/oxide interfaces.⁵²

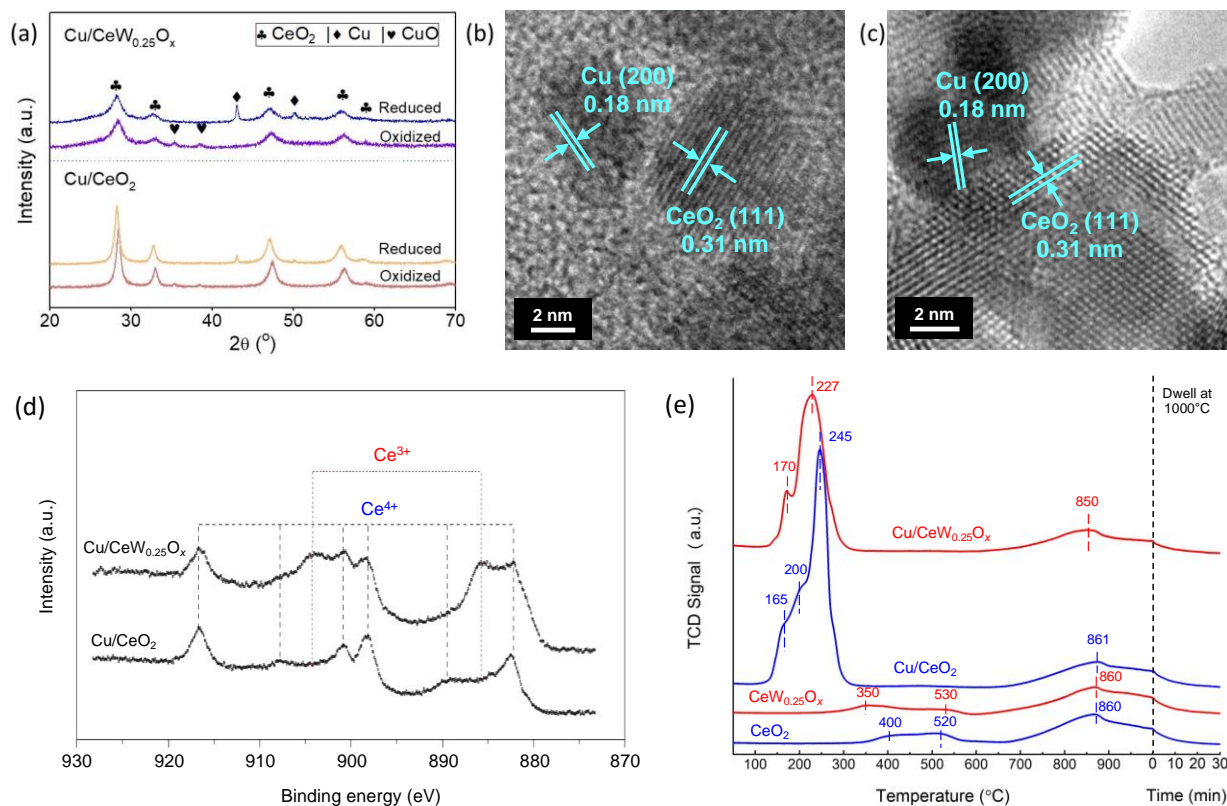


Figure 1. Ex situ characterisation of the as-prepared supports and Cu-loaded catalysts. (a): XRD patterns of the reduced and the oxidised catalysts. (b) and (c): HRTEM images of Cu/CeO₂ and Cu/CeW_{0.25}O_x, respectively. (d) High-resolution XPS spectra of Ce 3d. (e) H₂-TPR profiles of the air-calcined bare catalyst supports and the Cu loaded catalysts.

The reducibility of the air-calcined CeO₂ support and the Cu-loaded catalysts are investigated by H₂-TPR, as shown in Figure 1e. Three types of TPR peaks can be seen. Firstly, the low temperature peaks (≤ 200 °C) correspond to the reduction of CuO to metallic Cu.⁶¹ Secondly, the intermediate temperature (200 – 600 °C) peaks are assigned to the removal of oxygen from the surface of the CeO₂ supports.⁶² Lastly, the high temperature peaks (> 600 °C) can be assigned to

the removal of bulk lattice oxygen from CeO₂.⁶³ After Cu loading, the intermediate-temperature TPR peaks (350 – 530 °C) associated with the reduction of surface CeO₂ shift to lower temperatures, showing intense peaks around 227 – 245 °C, probably because Cu catalyses the reduction of CeO₂ by facilitating hydrogen spill-over. Upon W-doping, the main TPR peak associated with the removal of lattice oxygen from the surface of the fully oxidised CeO₂, shifts from 245 °C (in the case of Cu/CeO₂) to 227 °C (for Cu/CeW_{0.25}O_x), suggesting that the addition of W might have promoted the catalyst's ability to activate H₂. Although Cu/CeW_{0.25}O_x has substantially higher Ce³⁺ concentration, its overall reducibility, as shown by the total areas of the TPR peaks, does not appear significantly different from Cu/CeO₂; this observation agrees with the catalyst design hypothesis outlined in the Introduction.

3.2. CO₂ hydrogenation performance and mechanism

As shown in [Figure 2](#), the CO₂ hydrogenation activity of Cu/CeW_{0.25}O_x, evaluated at 250 °C and 35 bar, in a 23:69:8 mixture of CO₂:H₂:N₂, was substantially higher and more selective towards methanol than the unmodified Cu/CeO₂. On average, the unmodified Cu/CeO₂ showed a space-time yield (STY) of 1.26 mol_{MeOH}·kg_{cat}⁻¹·h⁻¹, a CO₂ conversion of 1.3% and a methanol selectivity of 51%. The STY of the Cu/CeO₂ catalyst is comparable to the other Cu/CeO₂-type catalysts reported in the literature (i.e. with STY varying in the range of 0.6 – 2.9 mol_{MeOH}·kg_{cat}⁻¹·h⁻¹), as shown in [Table S2](#). In contrast, the Cu/CeW_{0.25}O_x catalysts exhibited a one order of magnitude increase in STY (12.3 mol_{MeOH}·kg_{cat}⁻¹·h⁻¹), as well as significantly improved CO₂ conversion and methanol selectivity of 13% and 87%, respectively. The standard errors of the mean STY and mean selectivity, estimated over 72 h time-on-stream (TOS, see [Figure S5](#)) were both well below 1%. Given that Cu/CeO₂ and Cu/CeW_{0.25}O_x have comparable specific surface areas (105 and 84 m² g⁻¹, respectively), Cu loadings (9.8 wt% and 10.9 wt%, respectively), Cu chemical states (see

AES in Figure S4), Cu dispersion (see Table S1), and Cu particle sizes, such significant improvement in methanol synthesis activity of the Cu/CeW_{0.25}O_x catalyst over Cu/CeO₂ can only be explained by changes in the catalytic structure and, or possibly a change in the dominating reaction pathway. Additionally, the Cu/CeO₂ and Cu/CeW_{0.25}O_x catalysts showed stable performances over 72 h TOS (Figure S5), suggesting satisfactory stabilities. In comparison, we note that a Cu/WO₃ catalyst (results not shown) prepared by impregnating 10 wt% Cu on WO₃ showed no detectable CO₂ hydrogenation activity at 250 °C and 35 bar, suggesting that the Cu/WO₃ interfaces, even if it was present on Cu/CeW_{0.25}O_x, was not responsible for the observed catalytic enhancement.

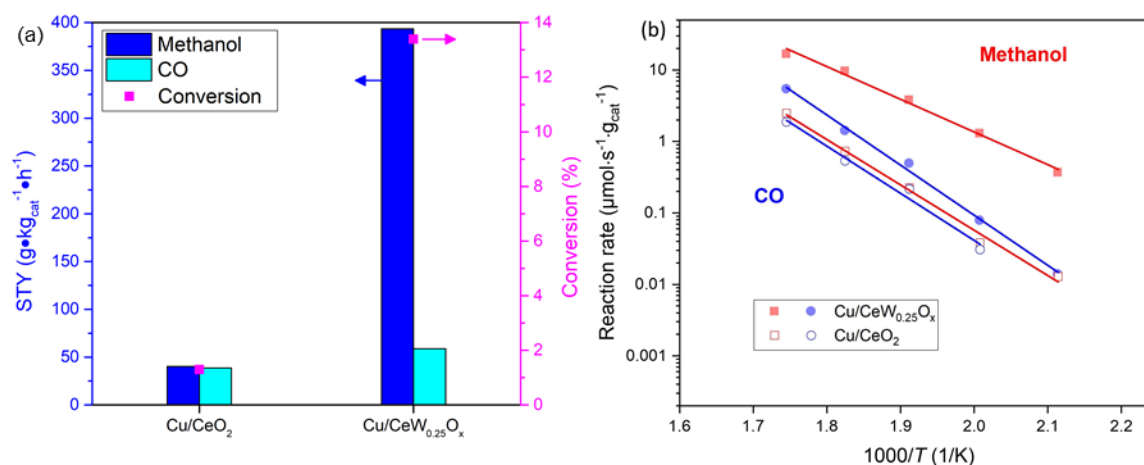


Figure 2. (a) Methanol STY and CO₂ conversion over Cu/CeO₂, and Cu/CeW_{0.25}O_x in a 23:69:8 mixture of CO₂/H₂/N₂ at 250 °C, 35 bar total pressure, with WHSV of 15000 mL g_{cat}⁻¹ h⁻¹. The error bars for methanol selectivity, calculated based on the data variability during the 72 h TOS experiments, are too small to be shown. (b) Arrhenius plots of the rate of CO and methanol formation over the Cu/CeO₂ and Cu/CeW_{0.25}O_x catalysts under the same operating conditions as (a), except the varied reaction temperatures.

Arrhenius analyses of the apparent rates of formation of methanol and CO are shown in [Figure 2b](#). All rate measurements were taken under differential reactor conditions, in which the catalyst weight and total flow rate were adjusted accordingly to keep the CO₂ conversion below 10%. For Cu/CeO₂, the apparent activation energies of the formation of CO and methanol are similar, i.e. $\sim 55 \text{ kJ} \pm 5 \text{ mol}^{-1}$ (see [Table S3](#), Supporting Information); this agrees with the understanding that methanol is formed, on Cu/CeO₂, via the RWGS pathway, with CO being a key intermediate.³⁰ Desorption of CO competes with its further hydrogenation, resulting in low methanol selectivity. For Cu/CeW_{0.25}O_x, the apparent activation energies of methanol formation and CO formation are 38 ± 2 and $58 \pm 2 \text{ kJ mol}^{-1}$, respectively ([Table S3](#), Supporting Information). This disparity in activation energy suggests that RWGS is unlikely to be the rate-controlling step for methanol formation on Cu/CeW_{0.25}O_x.

The catalytic mechanism of CO₂ hydrogenation was investigated by in situ DRIFTS, the results of which are shown in [Figure 3](#). After 30 min of CO₂ hydrogenation at 250 °C, 35 bar, the surface of Cu/CeW_{0.25}O_x showed adsorbates including adsorbed CO (2077 cm⁻¹), formate (the peaks at 1601, 1378, 1078 and 2842 cm⁻¹ correspond to the symmetric vibration of $\nu(\text{OCO})$, the asymmetric vibration $\nu_s(\text{OCO})$, the stretching vibration of -OCH and the stretching of -CH, respectively), carbonates (1432 cm⁻¹), HOCO ($\sim 1580 \text{ cm}^{-1}$) and possibly trace amount of HCO₃⁻ (1622 and 1222 cm⁻¹).⁶⁴ The low intensity of the CO peak at 2077 cm⁻¹ suggests that CO adsorption on Cu is indeed weak.^{65,66} After purging the reaction cell with He for 120 min, the adsorption peaks of CO and HCO₃⁻ disappeared owing to their weak adsorption. Then, H₂ was supplied to the purged reaction cell to hydrogenate the remaining adsorbates. From the time-resolved DRIFTS spectra, it can be seen that the intensity of the formate peaks decreased gradually over time, accompanied by the emergence of characteristic peaks corresponding to surface methoxy species at 2924 cm⁻¹, 2796

cm^{-1} and 1064 cm^{-1} .²¹ The observation of the methoxy group as a surface-significant species, in conjunction with the increase in methanol yield, suggests that methoxy is a key intermediate for methanol formation, in agreement with the literature.⁵² The dynamic spectral changes indicate that methanol is formed via the formate pathway on $\text{Cu/CeW}_{0.25}\text{O}_x$.

On Cu/CeO_2 , the same surface adsorbates were observed during steady-state hydrogenation (viz. CO , HCOO and HCO_3). After purging with He, HCOO is the main surface-significant species, as shown in Figure S6. However, the formate peaks remained largely unchanged over 300 min of continuous H_2 treatment at $250 \text{ }^\circ\text{C}$, 35 bar. Therefore, formate appears to act as a spectator on undoped Cu/CeO_2 , a phenomenon that has been previously reported in the literature.³⁰

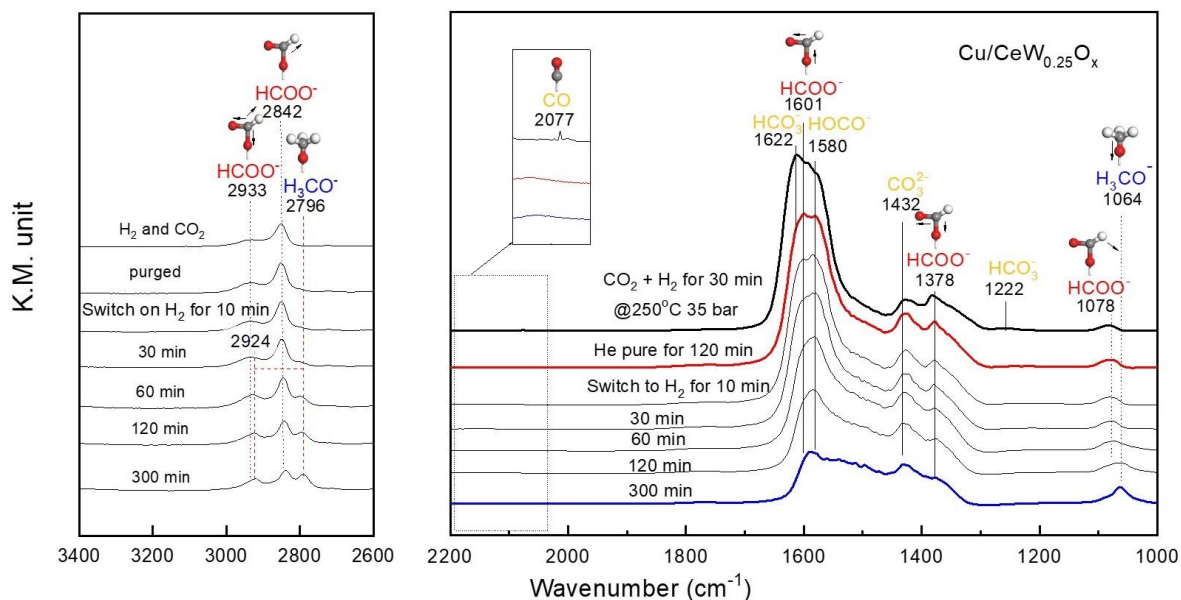


Figure 3. DRIFTS spectra recorded over $\text{Cu/CeW}_{0.25}\text{O}_x$ when the catalyst was exposed to CO_2 hydrogenation conditions for 30 min, followed by He purging for 120 min, and then treated with H_2 only. All measurements were performed at 35 bar total pressure at $250 \text{ }^\circ\text{C}$.

3.3. The roles of oxygen vacancies and Ce^{3+} sites

On undoped CeO₂, the presence of Ce³⁺ is often associated with the presence of oxygen vacancies, which in turn, is correlated to the redox activity of CeO₂ or the metal/CeO₂ interface. This is not the case for Cu/CeW_{0.25}O_x. In the following, we experimentally verify the lack of correlation between Ce³⁺, oxygen vacancies and redox activity on Cu/CeW_{0.25}O_x. First, CO₂-TPD was performed to probe the CO₂ affinity and the redox activity of the catalysts, as shown in [Figure 4](#). Over the unmodified CeO₂ support, a CO₂ desorption peak at 140 °C, with a shoulder at ~240 °C was observed, whereas a second CO₂ desorption peak can be seen ~760 °C. Upon W-doping, the shoulder peak ~240 °C shifted to ~320 °C, suggesting stronger CO₂ adsorption. The high temperature CO₂ desorption peaks ($m/z = 44$) above 700 °C are accompanied by CO desorption peaks ($m/z = 28$, after correcting for the $m/z = 28$ contribution by CO₂ fragmentation). The CO produced is attributed to the dissociative adsorption of CO₂ at an oxygen vacancy site.⁶⁷ Therefore, the amount of CO produced is indicative of the amount of redox-active oxygen vacancies (i.e. the oxygen vacancies that could reversibly form and disappear upon reduction and oxidation, respectively) present in the surface-region of the catalyst. To complement, we define the non-redox-active oxygen vacancies to be those originating from the inherent defects of the structures of the metal oxides. Therefore, the amount of non-redox-active oxygen vacancies would remain largely unchanged over varying redox environments. Accordingly, the quantifications of the redox-active oxygen vacancies are shown in [Table S4](#). The fact that Cu/CeW_{0.25}O_x and CeW_{0.25}O_x produced less CO than Cu/CeO₂ and CeO₂ suggests W-doping suppresses the redox activity of CeO₂, with or without Cu loading. This also agrees well with the O₂-TPO results, as shown in [Figure S7](#), i.e. pre-reduced CeO₂ consumes more O₂ (452 μmol/g) and is more redox-active than the pre-reduced CeW_{0.25}O_x (with an oxygen consumption of 283 μmol/g).

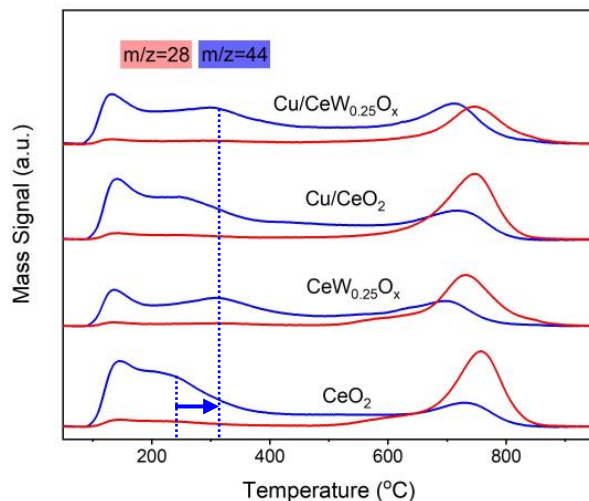


Figure 4. CO₂-TPD profiles of the CeO₂-based supports and the Cu loaded catalysts. The vertical blue lines indicate the shift of the CO₂ desorption peak.

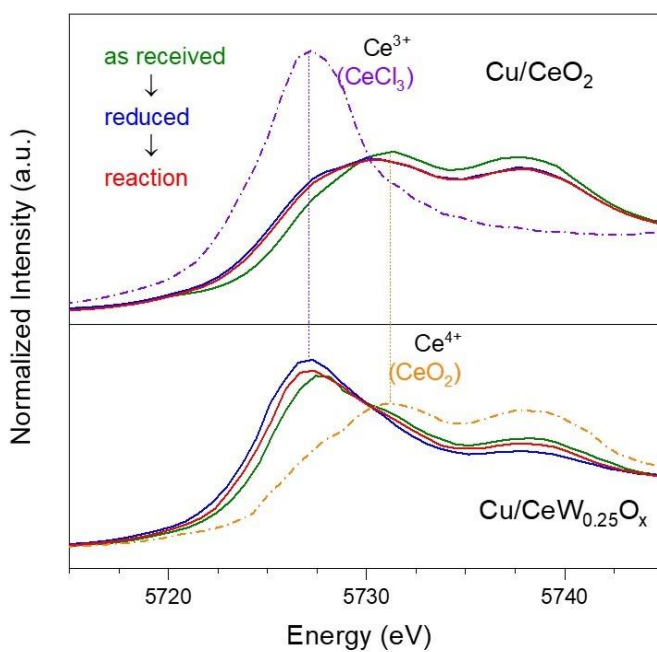


Figure 5. In situ XANES spectra of Ce L_{III} edge of the catalysts when freshly calcined (“as received”, green line), after reduction in 10% H₂/He at 500 °C, 10 bar for 30 min (“reduced”, blue line), and during CO₂ hydrogenation in a 23:69:8 mixture of CO₂/H₂/N₂ at 250 °C, 10 bar, after 30

min TOS (“reaction”, red line). The purple and orange dash-dot line refer to Ce^{3+} (CeCl_3) and Ce^{4+} (CeO_2) references, respectively.

The relative concentrations of Ce^{3+} and Ce^{4+} under pressurised CO_2 hydrogenation conditions were studied by in situ XANES, the results of which are shown in [Figure 5](#). By performing linear combination fitting (LCF) of the XANES data, the mole fraction of Ce^{3+} (balanced by Ce^{4+}) in the catalysts can be estimated. The results of the LCF analyses are shown in [Table S5](#) and discussed below. The air calcined CuO/CeO_2 catalyst precursor exhibits a typical Ce-L_{III} edge matching that of the reference CeO_2 , showing 0% Ce^{3+} . H_2 treatment at 500 °C resulted in the formation of oxygen vacancies and 17% Ce^{3+} , as Ce-L_{III} edge of the reduced Cu/CeO_2 catalyst moved to a lower energy. Under in situ CO_2 hydrogenation conditions at 250 °C and 10 bar total pressure, the reduced CeO_2 was slightly oxidised by the adsorbed CO_2 to produce CO ,^{39,40} accompanied by the elimination of a small fraction of oxygen vacancies and a slight decrease in the mole fraction of Ce^{3+} from 17% to 15%.

Compared to Cu/CeO_2 , the Ce-L_{III} edge of $\text{Cu/CeW}_{0.25}\text{O}_x$ responds to changes in the gas environment differently. The $\text{CuO/CeW}_{0.25}\text{O}_x$ catalyst precursor, after calcination in air, already contains 49% Ce^{3+} . The Ce^{3+} content in air-calcined $\text{CuO/CeW}_{0.25}\text{O}_x$ corresponds well to the Ce:W ratio of 4:1 and the fact that each W^{6+} could reduce two adjacent Ce^{4+} to Ce^{3+} . H_2 reduction at 500 °C and CO_2 hydrogenation reaction at 250 °C further increased the mole fraction of Ce^{3+} to 69% and 59%, respectively, whilst creating additional oxygen vacancies in the catalysts. Here, the changes in the amount of Ce^{3+} under varying gas environments characterize the redox activity of the catalyst, subject to practical limitations: (i) XANES is not a surface-sensitive technique and

(ii) the measurements may not capture all the transient redox processes taking place.⁶⁸ Based on the trends observed, the bulk redox activities of Cu/CeO₂ and Cu/CeW_{0.25}O_x appears similar.

The in situ EXAFS data of the Cu-K edge of both catalysts are carefully fitted by a single Cu-Cu shell (see [Figure S8](#), Supporting Information). The fitting results suggest average Cu-Cu first shell coordination numbers of 9.1 and 9.5 for Cu/CeO₂ and Cu/CeW_{0.25}O_x, respectively ([Table S6](#), Supporting Information), with mean Cu particle sizes of 3.2 nm and 3.5 nm, respectively, assuming spherical particle shapes.⁶⁹ The particle sizes estimated by EXAFS are close to the size estimates by HRTEM and N₂O chemisorption analyses (i.e. ~ 4 nm).

The chemical states of the surface regions of the catalysts were probed in situ by NAP-XPS. The signal-to-noise ratio in the C 1s region of the measured XPS spectra was too low to perform any meaningful interpretation, whereas the Cu 2p, Ce 3d, O 1s and W 4f regions, shown in [Figure 6](#), were analysed in detail. The Cu 2p spectra of both Cu/CeO₂ and Cu/CeW_{0.25}O_x, when (i) freshly reduced, (ii) oxidised by CO₂ at RT and (iii) under CO₂ hydrogenation conditions at 250 °C ([Figures 6a and 6b](#)), show the predominance of Cu⁰ species in the surface regions of the catalysts under CO₂ hydrogenation conditions at 1.2 mbar, 250 °C. Given the similarity of the positions of the Cu⁰ peaks (933 eV) of the two catalyst samples, it is plausible that W-doping does not have a notable influence on the chemical state of the Cu⁰ sites; this agrees with the similar Cu Auger spectra of the two catalysts ([Figure S4](#)). After O₂ treatment, the surface regions (and quite possibly the bulk) of the Cu particles were oxidised to Cu²⁺ for both Cu/CeO₂ and Cu/CeW_{0.25}O_x, as shown in [Figure 6c](#). Likewise, the similar Cu 2p peaks of the oxidised Cu/CeO₂ and Cu/CeW_{0.25}O_x are in line with the complementary experimental observations that W-doped does not have a significant effect on the chemical state of Cu.

The Ce 3d XPS spectra, plotted in [Figures 6d](#) and [6e](#), show trends agreeing well with the in situ XANES results, i.e., the surface region of the W-doped catalyst contains significantly more Ce^{3+} , with only a small fraction of Ce^{3+} oxidisable by CO_2 (*viz.* in CO_2 at RT and $\text{CO}_2 + \text{H}_2$ at 250 °C). In all NAP-XPS measurements, the surface region of $\text{Cu/CeW}_{0.25}\text{O}_x$ consistently contained more Ce^{3+} than that of Cu/CeO_2 , signifying the reduction of Ce^{4+} to Ce^{3+} and the stabilisation of the Ce^{3+} by W-doping. On the other hand, the surface region of the reduced Cu/CeO_2 appears more redox active (the Ce^{3+} content changes from 28.2% to 15.6% by CO_2 oxidation) than that of $\text{Cu/CeW}_{0.25}\text{O}_x$ (the Ce^{3+} content changes from 40.8% to 38.3%). Therefore, although $\text{Cu/CeW}_{0.25}\text{O}_x$ has more Ce^{3+} in its surface region than Cu/CeO_2 , the majority of the Ce^{3+} species are not redox-active. It is plausible that these non-redox-active Ce^{3+} are responsible for the significantly enhanced methanol synthesis activity of $\text{Cu/CeW}_{0.25}\text{O}_x$.

The XPS in the O 2p region also correlates well with the Ce 3d spectra. For Cu/CeO_2 ([Figure 6f](#)), the peak at 529.3 eV (denoted as O_β) can be assigned to O^{2-} located near the Ce^{4+} ions,⁷⁰ whereas the peak at 531.5 eV (denoted as O_α) is assigned to the carbonate-like and hydroxy adsorbates on the oxygen vacancy sites.⁷¹ For $\text{Cu/CeW}_{0.25}\text{O}_x$ ([Figure 6g](#)), the peak at 530.5 eV (O_β) is assigned to O^{2-} located near the Ce^{3+} ions,^{70,72} accompanied by the small peak at 532.6 eV (O_α), which is characteristic of the adsorbate-related contribution associated with oxygen vacancies. Therefore, the apparent shifts in the binding energies of the O 1s XPS upon W-doping can be explained by the change from the Ce^{4+} -rich surface of the CeO_2 support to one that is rich in Ce^{3+} . Additionally, the ratio of $\text{O}_\alpha/\text{O}_\beta$ is indicative of the activity of the oxygen vacancy sites, which could adsorptively activate CO_2 and H_2O . Upon the introduction of CO_2 at RT, the $\text{O}_\alpha/\text{O}_\beta$ ratio increases from 0.54 to 0.82 on Cu/CeO_2 , accompanied by the emergence of a peak at 536.3 eV, which corresponds to gaseous CO_2 molecules ([Figure 6d](#)). In contrast, the $\text{O}_\alpha/\text{O}_\beta$ ratio on the

reduced Cu/CeW_{0.25}O_x hardly changes (~0.07) upon exposure to CO₂, suggesting that the oxygen vacancies on Cu/CeW_{0.25}O_x have rather lower activity; this is in good agreement with its low CO selectivity observed during CO₂ hydrogenation experiment (Figure 1) and the low redox activity observed by CO₂-TPD (Figure 4) and NAP-XPS of the Ce 3d region (Figure 6e). Figure 6h plots the W 4f XPS of the Cu/CeW_{0.25}O_x catalyst at various stages of the NAP-XPS experiment. With the exception of the fully oxidised Cu/CeW_{0.25}O_x (after exposure to O₂ at 500 °C), the catalyst under otherwise reduced or partially reduced states exhibits W 4f XPS peaks that are shifted to higher binding energies relative to the WO₃ reference. This observation is in agreement with the theoretical study by Hu and Metiu, who concluded that the W dopant in CeO₂ would donate electrons to neighbouring Ce⁴⁺ species, forming Ce³⁺ sites.⁴² The charge transfer from W⁶⁺ to Ce³⁺ also corroborated by the NAP-XPS data of the Ce 3d region (Figure 6d). In addition, the effect of W dopant on the charge transfer mechanism is supported by H₂-TPR (Figure 1e), which portrays a negative shift in H₂ reduction temperature of CeW_{0.25}O_x after air calcination, indicating higher reducibility of CeW_{0.25}O_x as compared to CeO₂.

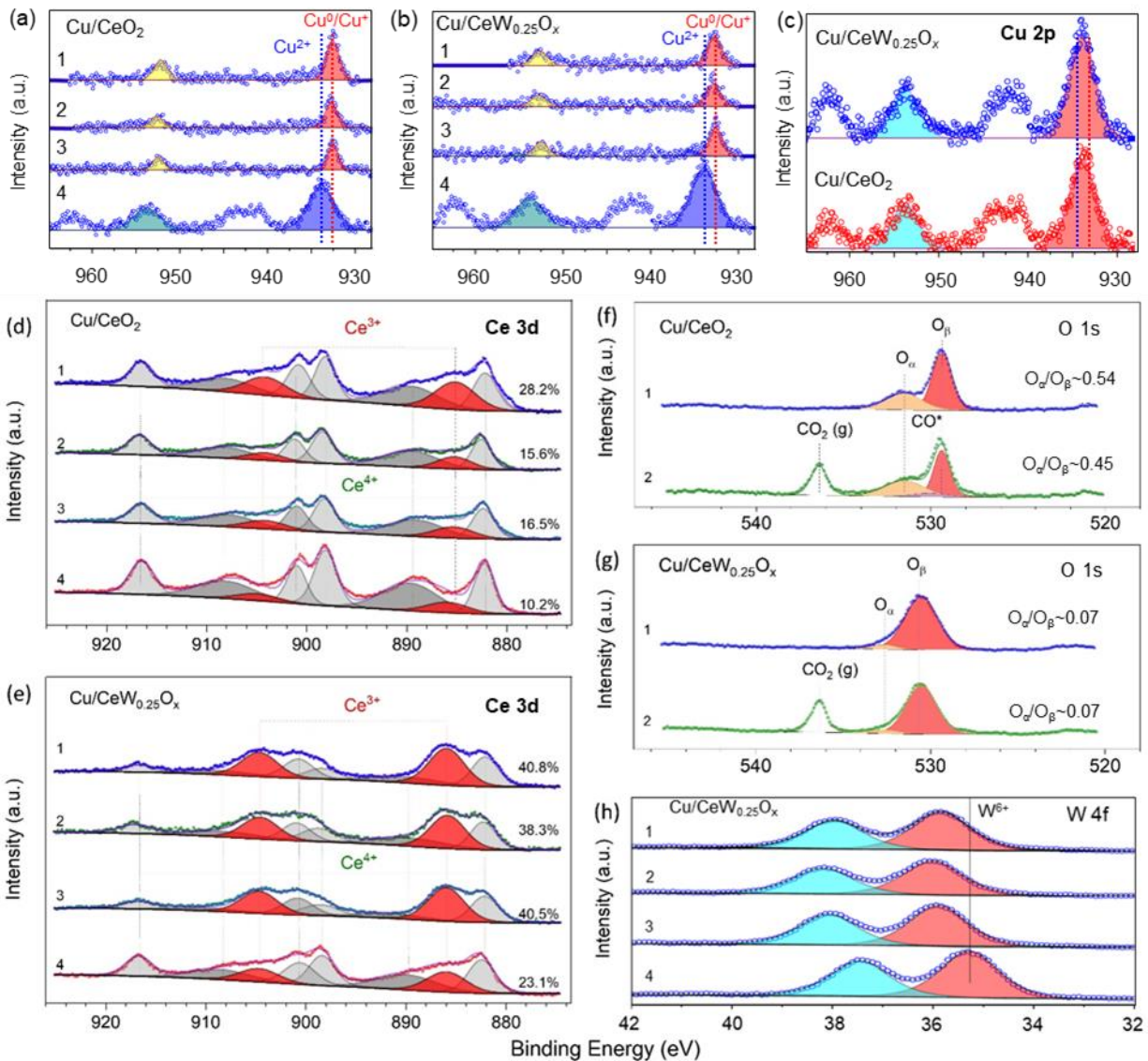


Figure 6. High-resolution XPS spectra obtained during the NAP-XPS experiments. (a) and (b) show the Cu 2p region. (c) shows the close inspection of the Cu 2p spectra after oxidation. (d) and (e) show the Ce 3d region, with the fractions of Ce³⁺ in the surface regions of the catalysts labelled on the right of each spectrum. (f) and (g) show the O 1s region. (h) shows the W 4f region; the dashed vertical line denotes the reference binding energy of WO₃. XPS measurements were taken when each sample was subjected to the following environments, in chronological order, 1)

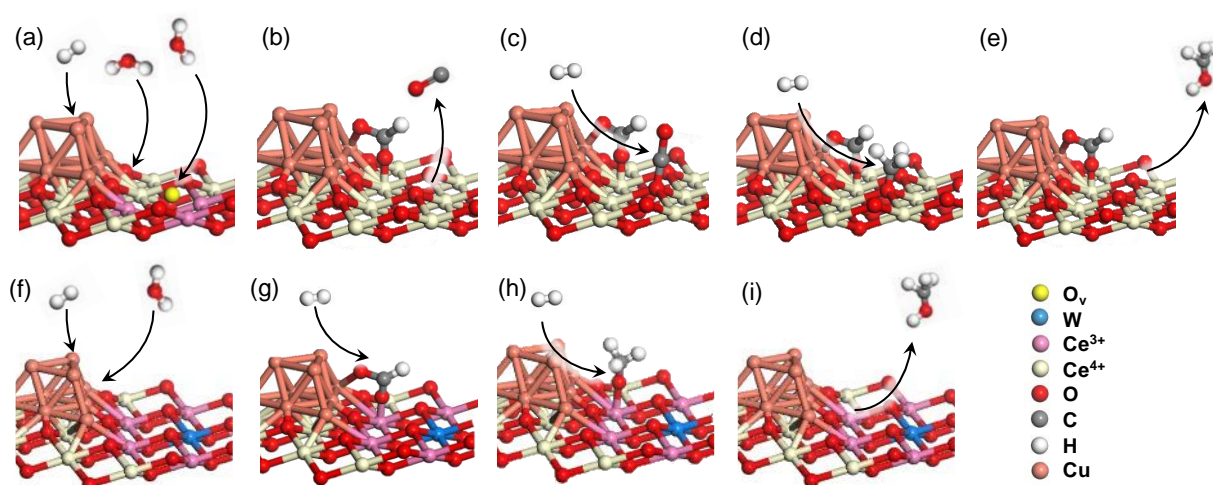
“reduced”: 0.4 mbar H₂ at 500 °C, 2) “CO₂ RT”: 0.5 mbar CO₂ at RT, 3) “CO₂+H₂ @250”: 0.3 mbar CO₂ and 0.9 mbar H₂ at 250 °C and 4) “oxidised”: 0.4 mbar O₂ at 500 °C.

Based on the experimental results discussed above, the catalytic consequences of W-doping are summarized in the following: (i) reducing Ce⁴⁺ to Ce³⁺ and stabilising Ce³⁺ both in the surface region and the bulk of the Cu/CeW_{0.25}O_x catalyst, (ii) suppressing the redox activity of the Cu/CeW_{0.25}O_x catalyst, (iii) promoting the formate pathway for CO₂ hydrogenation to methanol, and (iv) improving both CO₂ activation and selectivity towards methanol. Accordingly, the structural-functional relationship of the W-doped Cu/CeW_{0.25}O_x catalyst, is depicted in [Scheme 1](#) and elaborated below.

During CO₂ hydrogenation on unmodified Cu/CeO₂, the Cu nanoparticles facilitate hydrogen activation (including H₂ spill-over, [Scheme 1a](#)), whilst the redox-active oxygen vacancies formed on CeO₂ promote the dissociative activation of CO₂ to CO, i.e., RWGS via the Mars-van Krevelen (MvK) mechanism ([Scheme 1b](#)). Concomitantly, a fraction of the catalyst surface (possibly on the Cu and at the Cu/CeO₂ interfaces^{30,73–75}) is covered by formate spectators ([Scheme 1a](#)). As such, the formation of CO, with an apparent activation energy of 55 kJ mol⁻¹, is the rate limiting step for methanol formation on unmodified Cu/CeO₂. While the hydrogen of adsorbed CO produces methanol ([Scheme 1c-e](#)) The weak adsorption of CO on Cu results in low methanol selectivity and productivity.

For Cu/CeW_{0.25}O_x, the W dopants donate electrons to the neighbouring Ce⁴⁺, generating and stabilising substantial amount of non-redox-active Ce³⁺ ([Scheme 1f](#)). The lack of reducibility of Ce³⁺ and W⁶⁺, as shown by the NAP-XPS spectra in [Figures 6e](#) and [6h](#), hinders the ability of Cu/CeW_{0.25}O_x to lose lattice oxygen and create redox-active oxygen vacancies under CO₂

hydrogenation conditions, thus suppressing its redox activity. Consequently, RWGS and CO selectivity are effectively suppressed. Furthermore, the presence of the W-stabilised, non-redox-active Ce^{3+} species in the $\text{Cu}/\text{CeW}_{0.25}\text{O}_x$ catalyst promote the hydrogenation of the surface formate species (Scheme 1g), activating the formate pathway to become the dominant reaction pathway (Scheme 1h-i) with a significantly reduced apparent activation energy of 38 kJ mol^{-1} and a 10-fold increase in methanol STY.



Scheme 1. Proposed reaction mechanisms for CO_2 hydrogenation on (a – e) unmodified Cu/CeO_2 and (f – i) $\text{Cu}/\text{CeW}_{0.25}\text{O}_x$ and. The key steps on Cu/CeO_2 include: (a) activation of H_2 on Cu with hydrogen spillover across the Cu/CeO_2 interface, activation of CO_2 at the Cu/CeO_2 interface, and activation of CO_2 on an oxygen vacancy (O_v) of CeO_2 ; (b) desorption of CO produced by the dissociative adsorption of CO_2 at an oxygen vacancy, leaving behind formate spectators; (c) successive hydrogenation of adsorbed $^*\text{CO}$ species to form methoxy; (d) hydrogenation of surface methoxy species forming methanol; (e) desorption of methanol, leaving behind surface formate spectators. The key steps on $\text{Cu}/\text{CeW}_{0.25}\text{O}_x$ include: (f) activation of H_2 on Cu with hydrogen spillover across the Cu/CeO_2 interface and activation of CO_2 at the $\text{Cu}/\text{CeW}_{0.25}\text{O}_x$ interface; (g)

successive hydrogenation of formate species at the Cu/CeW_{0.25}O_x interface to form surface methoxy species; (h) hydrogenation of surface methoxy species to form methanol; (i) desorption of methanol.

The proposed structural-functional relationship is in line with the study by Senanayake et al,⁷⁶ who correlated the surface concentration of stable Ce³⁺ to the apparent rate of methanol formation. The improved CO₂ conversion with increasing Ce³⁺ is also corroborated by previous studies reporting that the Ce³⁺ sites on CeO₂ are responsible for the adsorptive activation of CO₂.⁷⁷⁻⁷⁹ However, the mechanistic function of the W-stabilised Ce³⁺ during the Cu-catalysed CO₂ hydrogenation is not fully understood and merits in-depth investigations in future studies, preferably with the help of theoretical tools such as density-functional theory calculations.

4. CONCLUSIONS

We prepared a Cu/CeW_{0.25}O_x catalyst for CO₂ hydrogenation to produce methanol. W-doping increases and stabilises the concentration of non-redox-active Ce³⁺ on Cu/CeW_{0.25}O_x, resulting in significantly enhanced methanol productivity and selectivity. The W-induced reduction of Ce⁴⁺ also uncouples the catalytic roles of oxygen vacancies and that of the Ce³⁺ species. On unmodified Cu/CeO₂, CO₂ is activated either (i) dissociatively at a redox-active oxygen vacancy on CeO₂, forming a weakly adsorbing *CO or (ii) forming a stable formate spectator. Subsequently, CO₂ is hydrogenated via the RWGS pathway with inherently low methanol selectivity. In comparison, W-doping resulted in a considerably reduced CeO₂ surface having low redox activity and suppressed CO selectivity. This is achieved by W donating electrons to neighboring Ce⁴⁺, reducing them to Ce³⁺ without generating additional oxygen vacancies. The abundant non-redox-active Ce³⁺ species on Cu/CeW_{0.25}O_x promote the hydrogenation of formate to produce methanol at a rate that is 10 times faster than undoped Cu/CeO₂. Beyond CO₂ hydrogenation, high-valency cation doping

may be further exploited as a means to tune the catalytic activity of CeO₂ for reactions where high redox activity is undesired.

ASSOCIATED CONTENT

Supporting Information.

The following files are available free of charge.

Supporting information.pdf (PDF)

AUTHOR INFORMATION

Corresponding Author

* Wen Liu, School of Chemical and Biomedical Engineering, Nanyang Technological University, 62 Nanyang Drive, Singapore 637459, Singapore. Email: wenliu@ntu.edu.sg

Author Contributions

The manuscript was written through contributions of all authors. All authors have given approval to the final version of the manuscript.

Funding Sources

National Research Foundation of Singapore: Campus for Research Excellence and Technological Enterprise (CREATE) programme.

Ministry of Education, Singapore: Academic Research Funding Tier 1: RT03/19

ACKNOWLEDGMENT

This research is funded by the National Research Foundation (NRF), Prime Minister's Office, Singapore under its Campus for Research Excellence and Technological Enterprise (CREATE) programme and Ministry of Education, Singapore under its AcRF Tier 1 (RT03/19). The authors would also like to thank Prof. Kongzhai Li from Kunming University of Science and Technology for the helpful discussions.

REFERENCES

- (1) Cuéllar-Franca, R. M.; Azapagic, A. Carbon Capture, Storage and Utilisation Technologies: A Critical Analysis and Comparison of Their Life Cycle Environmental Impacts. *Journal of CO₂ Utilization* **2015**, *9*, 82–102. <https://doi.org/10.1016/j.jcou.2014.12.001>.
- (2) Bui, M.; Adjiman, C. S.; Bardow, A.; Anthony, E. J.; Boston, A.; Brown, S.; Fennell, P. S.; Fuss, S.; Galindo, A.; Hackett, L. A.; Hallett, J. P.; Herzog, H. J.; Jackson, G.; Kemper, J.; Krevor, S.; Maitland, G. C.; Matuszewski, M.; Metcalfe, I. S.; Petit, C.; Puxty, G.; Reimer, J.; Reiner, D. M.; Rubin, E. S.; Scott, S. A.; Shah, N.; Smit, B.; Trusler, J. P. M.; Webley, P.; Wilcox, J.; Dowell, N. M. Carbon Capture and Storage (CCS): The Way Forward. *Energy Environ. Sci.* **2018**, *11* (5), 1062–1176. <https://doi.org/10.1039/C7EE02342A>.
- (3) Kätelhön, A.; Meys, R.; Deutz, S.; Suh, S.; Bardow, A. Climate Change Mitigation Potential of Carbon Capture and Utilization in the Chemical Industry. *PNAS* **2019**, *116* (23), 11187–11194. <https://doi.org/10.1073/pnas.1821029116>.
- (4) Rissman, J.; Bataille, C.; Masanet, E.; Aden, N.; Morrow, W. R.; Zhou, N.; Elliott, N.; Dell, R.; Heeren, N.; Huckestein, B.; Cresko, J.; Miller, S. A.; Roy, J.; Fennell, P.; Cremmins, B.; Koch Blank, T.; Hone, D.; Williams, E. D.; de la Rue du Can, S.; Sisson, B.; Williams, M.; Katzenberger, J.; Burtraw, D.; Sethi, G.; Ping, H.; Danielson, D.; Lu, H.; Lorber, T.; Dinkel, J.; Helseth, J. Technologies and Policies to Decarbonize Global Industry: Review and Assessment of Mitigation Drivers through 2070. *Applied Energy* **2020**, *266*, 114848. <https://doi.org/10.1016/j.apenergy.2020.114848>.
- (5) Tao, L.; Choksi, T. S.; Liu, W.; Pérez-Ramírez, J. Synthesizing High-Volume Chemicals from CO₂ without Direct H₂ Input. *ChemSusChem* *n/a* (n/a). <https://doi.org/10.1002/cssc.202001604>.
- (6) Burkart, M. D.; Hazari, N.; Tway, C. L.; Zeitler, E. L. Opportunities and Challenges for Catalysis in Carbon Dioxide Utilization. *ACS Catal.* **2019**, *9* (9), 7937–7956. <https://doi.org/10.1021/acscatal.9b02113>.
- (7) Jia, C.; Gao, J.; Dai, Y.; Zhang, J.; Yang, Y. The Thermodynamics Analysis and Experimental Validation for Complicated Systems in CO₂ Hydrogenation Process. *Journal of Energy Chemistry* **2016**, *25* (6), 1027–1037. <https://doi.org/10.1016/j.jechem.2016.10.003>.
- (8) Yang, M.; Fan, D.; Wei, Y.; Tian, P.; Liu, Z. Recent Progress in Methanol-to-Olefins (MTO) Catalysts. *Advanced Materials* **2019**, *31* (50), 1902181. <https://doi.org/10.1002/adma.201902181>.

- (9) Ashok, J.; Falbo, L.; Das, S.; Dewangan, N.; Visconti, C. G.; Kawi, S. Catalytic CO₂ Conversion to Added-Value Energy Rich C1 Products. *An Economy Based on Carbon Dioxide and Water* **2019**, 155–210. https://doi.org/10.1007/978-3-030-15868-2_5.
- (10) Tountas, A. A.; Peng, X.; Tavasoli, A. V.; Duchesne, P. N.; Dingle, T. L.; Dong, Y.; Hurtado, L.; Mohan, A.; Sun, W.; Ulmer, U.; Wang, L.; Wood, T. E.; Maravelias, C. T.; Sain, M. M.; Ozin, G. A. Towards Solar Methanol: Past, Present, and Future. *Advanced Science* **2019**, 6 (8), 1801903. <https://doi.org/10.1002/advs.201801903>.
- (11) González-Garay, A.; Frei, M. S.; Al-Qahtani, A.; Mondelli, C.; Guillén-Gosálbez, G.; Pérez-Ramírez, J. Plant-to-Planet Analysis of CO₂-Based Methanol Processes. *Energy Environ. Sci.* **2019**, 12 (12), 3425–3436. <https://doi.org/10.1039/C9EE01673B>.
- (12) Tackett, B. M.; Gomez, E.; Chen, J. G. Net Reduction of CO₂ via Its Thermocatalytic and Electrocatalytic Transformation Reactions in Standard and Hybrid Processes. *Nature Catalysis* **2019**, 2 (5), 381. <https://doi.org/10.1038/s41929-019-0266-y>.
- (13) Sehested, J. Industrial and Scientific Directions of Methanol Catalyst Development. *Journal of Catalysis* **2019**, 371, 368–375. <https://doi.org/10.1016/j.jcat.2019.02.002>.
- (14) Olah, G. A. Towards Oil Independence Through Renewable Methanol Chemistry. *Angewandte Chemie International Edition* **2013**, 52 (1), 104–107. <https://doi.org/10.1002/anie.201204995>.
- (15) Liang, B.; Ma, J.; Su, X.; Yang, C.; Duan, H.; Zhou, H.; Deng, S.; Li, L.; Huang, Y. Investigation on Deactivation of Cu/ZnO/Al₂O₃ Catalyst for CO₂ Hydrogenation to Methanol. *Ind. Eng. Chem. Res.* **2019**, 58 (21), 9030–9037. <https://doi.org/10.1021/acs.iecr.9b01546>.
- (16) Zhong, J.; Yang, X.; Wu, Z.; Liang, B.; Huang, Y.; Zhang, T. State of the Art and Perspectives in Heterogeneous Catalysis of CO₂ Hydrogenation to Methanol. *Chem. Soc. Rev.* **2020**, 49 (5), 1385–1413. <https://doi.org/10.1039/C9CS00614A>.
- (17) Fujitani, T.; Saito, M.; Kanai, Y.; Watanabe, T.; Nakamura, J.; Uchijima, T. Development of an Active Ga₂O₃ Supported Palladium Catalyst for the Synthesis of Methanol from Carbon Dioxide and Hydrogen. *Applied Catalysis A: General* **1995**, 125 (2), L199–L202. [https://doi.org/10.1016/0926-860X\(95\)00049-6](https://doi.org/10.1016/0926-860X(95)00049-6).
- (18) Arena, F.; Mezzatesta, G.; Zafarana, G.; Trunfio, G.; Frusteri, F.; Spadaro, L. Effects of Oxide Carriers on Surface Functionality and Process Performance of the Cu–ZnO System in the Synthesis of Methanol via CO₂ Hydrogenation. *Journal of Catalysis* **2013**, 300, 141–151. <https://doi.org/10.1016/j.jcat.2012.12.019>.
- (19) Rui, N.; Wang, Z.; Sun, K.; Ye, J.; Ge, Q.; Liu, C. CO₂ Hydrogenation to Methanol over Pd/In₂O₃: Effects of Pd and Oxygen Vacancy. *Applied Catalysis B: Environmental* **2017**, 218, 488–497. <https://doi.org/10.1016/j.apcatb.2017.06.069>.
- (20) Bai, S.; Shao, Q.; Feng, Y.; Bu, L.; Huang, X. Highly Efficient Carbon Dioxide Hydrogenation to Methanol Catalyzed by Zigzag Platinum–Cobalt Nanowires. *Small* **2017**, 13 (22), 1604311. <https://doi.org/10.1002/sml.201604311>.
- (21) Wang, J.; Li, G.; Li, Z.; Tang, C.; Feng, Z.; An, H.; Liu, H.; Liu, T.; Li, C. A Highly Selective and Stable ZnO–ZrO₂ Solid Solution Catalyst for CO₂ Hydrogenation to Methanol. *Science Advances* **2017**, 3 (10), e1701290. <https://doi.org/10.1126/sciadv.1701290>.
- (22) Tsoukalou, A.; Abdala, P. M.; Stoian, D.; Huang, X.; Willinger, M.-G.; Fedorov, A.; Müller, C. R. Structural Evolution and Dynamics of an In₂O₃ Catalyst for CO₂

- Hydrogenation to Methanol: An Operando XAS-XRD and In Situ TEM Study. *J. Am. Chem. Soc.* **2019**, *141* (34), 13497–13505. <https://doi.org/10.1021/jacs.9b04873>.
- (23) Frei, M. S.; Mondelli, C.; García-Muelas, R.; Kley, K. S.; Puértolas, B.; López, N.; Safonova, O. V.; Stewart, J. A.; Curulla Ferré, D.; Pérez-Ramírez, J. Atomic - Scale Engineering of Indium Oxide Promotion by Palladium for Methanol Production via CO₂ Hydrogenation. *Nature Communications* **2019**, *10* (1), 1–11. <https://doi.org/10.1038/s41467-019-11349-9>.
- (24) Li, Y.; Chan, S. H.; Sun, Q. Heterogeneous Catalytic Conversion of CO₂: A Comprehensive Theoretical Review. *Nanoscale* **2015**, *7* (19), 8663–8683. <https://doi.org/10.1039/C5NR00092K>.
- (25) Kattel, S.; Liu, P.; Chen, J. G. Tuning Selectivity of CO₂ Hydrogenation Reactions at the Metal/Oxide Interface. *J. Am. Chem. Soc.* **2017**, *139* (29), 9739–9754. <https://doi.org/10.1021/jacs.7b05362>.
- (26) Nie, X.; Li, W.; Jiang, X.; Guo, X.; Song, C. Chapter Two - Recent Advances in Catalytic CO₂ Hydrogenation to Alcohols and Hydrocarbons. In *Advances in Catalysis*; Song, C., Ed.; Academic Press, 2019; Vol. 65, pp 121–233. <https://doi.org/10.1016/bs.acat.2019.10.002>.
- (27) Jiang, X.; Nie, X.; Guo, X.; Song, C.; Chen, J. G. Recent Advances in Carbon Dioxide Hydrogenation to Methanol via Heterogeneous Catalysis. *Chem. Rev.* **2020**. <https://doi.org/10.1021/acs.chemrev.9b00723>.
- (28) Bowker, M. Methanol Synthesis from CO₂ Hydrogenation. *ChemCatChem* **2019**, *11* (17), 4238–4246. <https://doi.org/10.1002/cctc.201900401>.
- (29) Dang, S.; Yang, H.; Gao, P.; Wang, H.; Li, X.; Wei, W.; Sun, Y. A Review of Research Progress on Heterogeneous Catalysts for Methanol Synthesis from Carbon Dioxide Hydrogenation. *Catalysis Today* **2019**, *330*, 61–75. <https://doi.org/10.1016/j.cattod.2018.04.021>.
- (30) Graciani, J.; Mudiyanse, K.; Xu, F.; Baber, A. E.; Evans, J.; Senanayake, S. D.; Stacchiola, D. J.; Liu, P.; Hrbek, J.; Sanz, J. F.; Rodriguez, J. A. Highly Active Copper-Ceria and Copper-Ceria-Titania Catalysts for Methanol Synthesis from CO₂. *Science* **2014**, *345* (6196), 546–550. <https://doi.org/10.1126/science.1253057>.
- (31) A. Rodriguez, J.; C. Grinter, D.; Liu, Z.; M. Palomino, R.; D. Senanayake, S. Ceria-Based Model Catalysts: Fundamental Studies on the Importance of the Metal–Ceria Interface in CO Oxidation, the Water–Gas Shift, CO₂ Hydrogenation, and Methane and Alcohol Reforming. *Chemical Society Reviews* **2017**, *46* (7), 1824–1841. <https://doi.org/10.1039/C6CS00863A>.
- (32) Vilé, G.; Colussi, S.; Krumeich, F.; Trovarelli, A.; Pérez-Ramírez, J. Opposite Face Sensitivity of CeO₂ in Hydrogenation and Oxidation Catalysis. *Angewandte Chemie International Edition* **2014**, *53* (45), 12069–12072. <https://doi.org/10.1002/anie.201406637>.
- (33) Trovarelli, A.; Llorca, J. Ceria Catalysts at Nanoscale: How Do Crystal Shapes Shape Catalysis? *ACS Catal.* **2017**, *7* (7), 4716–4735. <https://doi.org/10.1021/acscatal.7b01246>.
- (34) Montini, T.; Melchionna, M.; Monai, M.; Fornasiero, P. Fundamentals and Catalytic Applications of CeO₂-Based Materials. *Chem. Rev.* **2016**, *116* (10), 5987–6041. <https://doi.org/10.1021/acs.chemrev.5b00603>.
- (35) Schmitt, R.; Nanning, A.; Kraynis, O.; Korobko, R.; I. Frenkel, A.; Lubomirsky, I.; M. Haile, S.; M. Rupp, J. L. A Review of Defect Structure and Chemistry in Ceria and Its

- Solid Solutions. *Chemical Society Reviews* **2020**, *49* (2), 554–592.
<https://doi.org/10.1039/C9CS00588A>.
- (36) Xu, B.; Yang, H.; Zhang, Q.; Yuan, S.; Xie, A.; Zhang, M.; Ohno, T. Design and Synthesis of Sm, Y, La and Nd-Doped CeO₂ with a Broom-like Hierarchical Structure: A Photocatalyst with Enhanced Oxidation Performance. *ChemCatChem* **2020**, *12* (9), 2638–2646. <https://doi.org/10.1002/cctc.201902309>.
- (37) Jiang, S.; Zhang, R.; Liu, H.; Rao, Y.; Yu, Y.; Chen, S.; Yue, Q.; Zhang, Y.; Kang, Y. Promoting Formation of Oxygen Vacancies in Two-Dimensional Cobalt-Doped Ceria Nanosheets for Efficient Hydrogen Evolution. *J. Am. Chem. Soc.* **2020**, *142* (14), 6461–6466. <https://doi.org/10.1021/jacs.9b13915>.
- (38) Zhang, Z.; Wang, Y.; Lu, J.; Zhang, J.; Li, M.; Liu, X.; Wang, F. Pr-Doped CeO₂ Catalyst in the Prins Condensation–Hydrolysis Reaction: Are All of the Defect Sites Catalytically Active? *ACS Catal.* **2018**, *8* (4), 2635–2644. <https://doi.org/10.1021/acscatal.7b04500>.
- (39) Kumari, N.; Haider, M. A.; Agarwal, M.; Sinha, N.; Basu, S. Role of Reduced CeO₂(110) Surface for CO₂ Reduction to CO and Methanol. *J. Phys. Chem. C* **2016**, *120* (30), 16626–16635. <https://doi.org/10.1021/acs.jpcc.6b02860>.
- (40) Guo, C.; Wei, S.; Zhou, S.; Zhang, T.; Wang, Z.; Ng, S.-P.; Lu, X.; Wu, C.-M. L.; Guo, W. Initial Reduction of CO₂ on Pd-, Ru-, and Cu-Doped CeO₂(111) Surfaces: Effects of Surface Modification on Catalytic Activity and Selectivity. *ACS Appl. Mater. Interfaces* **2017**, *9* (31), 26107–26117. <https://doi.org/10.1021/acsami.7b07945>.
- (41) Chang, K.; Wang, T.; Chen, J. G. Hydrogenation of CO₂ to Methanol over CuCeTiO_x Catalysts. *Applied Catalysis B: Environmental* **2017**, *206*, 704–711. <https://doi.org/10.1016/j.apcatb.2017.01.076>.
- (42) Hu, Z.; Metiu, H. Effect of Dopants on the Energy of Oxygen-Vacancy Formation at the Surface of Ceria: Local or Global? *J. Phys. Chem. C* **2011**, *115* (36), 17898–17909. <https://doi.org/10.1021/jp205432r>.
- (43) Chang, K.; Zhang, H.; Cheng, M.; Lu, Q. Application of Ceria in CO₂ Conversion Catalysis. *ACS Catal.* **2019**, 613–631. <https://doi.org/10.1021/acscatal.9b03935>.
- (44) Guo, J.; Lou, H.; Mo, L.; Zheng, X. The Reactivity of Surface Active Carbonaceous Species with CO₂ and Its Role on Hydrocarbon Conversion Reactions. *Journal of Molecular Catalysis A: Chemical* **2010**, *316* (1), 1–7. <https://doi.org/10.1016/j.molcata.2009.09.023>.
- (45) Arena, F.; Mezzatesta, G.; Zafarana, G.; Trunfio, G.; Frusteri, F.; Spadaro, L. How Oxide Carriers Control the Catalytic Functionality of the Cu–ZnO System in the Hydrogenation of CO₂ to Methanol. *Catalysis Today* **2013**, *210*, 39–46. <https://doi.org/10.1016/j.cattod.2013.02.016>.
- (46) Angelo, L.; Girleanu, M.; Ersen, O.; Serra, C.; Parkhomenko, K.; Roger, A.-C. Catalyst Synthesis by Continuous Coprecipitation under Micro-Fluidic Conditions: Application to the Preparation of Catalysts for Methanol Synthesis from CO₂/H₂. *Catalysis Today* **2016**, *270*, 59–67. <https://doi.org/10.1016/j.cattod.2015.09.028>.
- (47) Tan, Q.; Shi, Z.; Wu, D. CO₂ Hydrogenation to Methanol over a Highly Active Cu–Ni/CeO₂–Nanotube Catalyst. *Ind. Eng. Chem. Res.* **2018**, *57* (31), 10148–10158. <https://doi.org/10.1021/acs.iecr.8b01246>.
- (48) Mureddu, M.; Ferrara, F.; Pettinau, A. Highly Efficient CuO/ZnO/ZrO₂@SBA-15 Nanocatalysts for Methanol Synthesis from the Catalytic Hydrogenation of CO₂. *Applied*

- Catalysis B: Environmental* **2019**, 258, 117941.
<https://doi.org/10.1016/j.apcatb.2019.117941>.
- (49) Deerattrakul, V.; Yigit, N.; Rupprechter, G.; Kongkachuichay, P. The Roles of Nitrogen Species on Graphene Aerogel Supported Cu-Zn as Efficient Catalysts for CO₂ Hydrogenation to Methanol. *Applied Catalysis A: General* **2019**, 580, 46–52.
<https://doi.org/10.1016/j.apcata.2019.04.030>.
- (50) Liu, T.; Hong, X.; Liu, G. In Situ Generation of the Cu@3D-ZrO_x Framework Catalyst for Selective Methanol Synthesis from CO₂/H₂. *ACS Catal.* **2020**, 10 (1), 93–102.
<https://doi.org/10.1021/acscatal.9b03738>.
- (51) Li, S.; Guo, L.; Ishihara, T. Hydrogenation of CO₂ to Methanol over Cu/AlCeO Catalyst. *Catalysis Today* **2020**, 339, 352–361. <https://doi.org/10.1016/j.cattod.2019.01.015>.
- (52) Xie, B.; Wong, R. J.; Tan, T. H.; Higham, M.; Gibson, E. K.; Decarolis, D.; Callison, J.; Aguey-Zinsou, K.-F.; Bowker, M.; Catlow, C. R. A.; Scott, J.; Amal, R. Synergistic Ultraviolet and Visible Light Photo-Activation Enables Intensified Low-Temperature Methanol Synthesis over Copper/Zinc Oxide/Alumina. *Nat Commun* **2020**, 11 (1), 1615.
<https://doi.org/10.1038/s41467-020-15445-z>.
- (53) Biesinger, M. C. Advanced Analysis of Copper X-Ray Photoelectron Spectra. *Surface and Interface Analysis* **2017**, 49 (13), 1325–1334. <https://doi.org/10.1002/sia.6239>.
- (54) Shan, W.; Liu, F.; He, H.; Shi, X.; Zhang, C. Novel Cerium–Tungsten Mixed Oxide Catalyst for the Selective Catalytic Reduction of NO_x with NH₃. *Chem. Commun.* **2011**, 47 (28), 8046–8048. <https://doi.org/10.1039/C1CC12168E>.
- (55) Chen, L.; Li, J.; Ablikim, W.; Wang, J.; Chang, H.; Ma, L.; Xu, J.; Ge, M.; Arandiyani, H. CeO₂–WO₃ Mixed Oxides for the Selective Catalytic Reduction of NO_x by NH₃ Over a Wide Temperature Range. *Catal Lett* **2011**, 141 (12), 1859–1864.
<https://doi.org/10.1007/s10562-011-0701-4>.
- (56) Kumar, P.; With, P.; Srivastava, V. C.; Gläser, R.; Mishra, I. M. Efficient Ceria-Zirconium Oxide Catalyst for Carbon Dioxide Conversions: Characterization, Catalytic Activity and Thermodynamic Study. *Journal of Alloys and Compounds* **2017**, 696, 718–726.
<https://doi.org/10.1016/j.jallcom.2016.10.293>.
- (57) Liu, B.; Li, C.; Zhang, G.; Yao, X.; Chuang, S. S. C.; Li, Z. Oxygen Vacancy Promoting Dimethyl Carbonate Synthesis from CO₂ and Methanol over Zr-Doped CeO₂ Nanorods. *ACS Catal.* **2018**, 8 (11), 10446–10456. <https://doi.org/10.1021/acscatal.8b00415>.
- (58) Fu, Z.; Zhong, Y.; Yu, Y.; Long, L.; Xiao, M.; Han, D.; Wang, S.; Meng, Y. TiO₂-Doped CeO₂ Nanorod Catalyst for Direct Conversion of CO₂ and CH₃OH to Dimethyl Carbonate: Catalytic Performance and Kinetic Study. *ACS Omega* **2018**, 3 (1), 198–207.
<https://doi.org/10.1021/acsomega.7b01475>.
- (59) Lin, L.; Yao, S.; Liu, Z.; Zhang, F.; Li, N.; Vovchok, D.; Martínez-Arias, A.; Castañeda, R.; Lin, J.; Senanayake, S. D.; Su, D.; Ma, D.; Rodriguez, J. A. In Situ Characterization of Cu/CeO₂ Nanocatalysts for CO₂ Hydrogenation: Morphological Effects of Nanostructured Ceria on the Catalytic Activity. *J. Phys. Chem. C* **2018**, 122 (24), 12934–12943. <https://doi.org/d>.
- (60) Reddy, B. M.; Khan, A.; Yamada, Y.; Kobayashi, T.; Loridant, S.; Volta, J.-C. Surface Characterization of CeO₂/SiO₂ and V₂O₅/CeO₂/SiO₂ Catalysts by Raman, XPS, and Other Techniques. *J. Phys. Chem. B* **2002**, 106 (42), 10964–10972.
<https://doi.org/10.1021/jp021195v>.

- (61) Lykaki, M.; Pachatouridou, E.; Carabineiro, S. A. C.; Iliopoulou, E.; Andriopoulou, C.; Kallithrakas-Kontos, N.; Boghosian, S.; Konsolakis, M. Ceria Nanoparticles Shape Effects on the Structural Defects and Surface Chemistry: Implications in CO Oxidation by Cu/CeO₂ Catalysts. *Applied Catalysis B: Environmental* **2018**, *230*, 18–28. <https://doi.org/10.1016/j.apcatb.2018.02.035>.
- (62) Peng, Y.; Li, K.; Li, J. Identification of the Active Sites on CeO₂–WO₃ Catalysts for SCR of NO_x with NH₃: An in Situ IR and Raman Spectroscopy Study. *Applied Catalysis B: Environmental* **2013**, *140–141*, 483–492. <https://doi.org/10.1016/j.apcatb.2013.04.043>.
- (63) Sepúlveda-Escribano, A.; Coloma, F.; Rodríguez-Reinoso, F. Promoting Effect of Ceria on the Gas Phase Hydrogenation of Crotonaldehyde over Platinum Catalysts. *Journal of Catalysis* **1998**, *178* (2), 649–657. <https://doi.org/10.1006/jcat.1998.2199>.
- (64) Vayssilov, G. N.; Mihaylov, M.; Petkov, P. St.; Hadjiivanov, K. I.; Neyman, K. M. Reassignment of the Vibrational Spectra of Carbonates, Formates, and Related Surface Species on Ceria: A Combined Density Functional and Infrared Spectroscopy Investigation. *J. Phys. Chem. C* **2011**, *115* (47), 23435–23454. <https://doi.org/10.1021/jp208050a>.
- (65) Bera, P.; Cámara, A. L.; Hornés, A.; Martínez-Arias, A. Comparative in Situ DRIFTS-MS Study of 12CO- and 13CO-TPR on CuO/CeO₂ Catalyst. *J. Phys. Chem. C* **2009**, *113* (24), 10689–10695. <https://doi.org/10.1021/jp9020504>.
- (66) Zhu, M.; Tian, P.; Kurtz, R.; Lunkenbein, T.; Xu, J.; Schlögl, R.; Wachs, I. E.; Han, Y.-F. Strong Metal–Support Interactions between Copper and Iron Oxide during the High-Temperature Water-Gas Shift Reaction. *Angewandte Chemie* **2019**, *131* (27), 9181–9185. <https://doi.org/10.1002/ange.201903298>.
- (67) Schweke, D.; Zalkind, S.; Attia, S.; Bloch, J. The Interaction of CO₂ with CeO₂ Powder Explored by Correlating Adsorption and Thermal Desorption Analyses. *J. Phys. Chem. C* **2018**, *122* (18), 9947–9957. <https://doi.org/10.1021/acs.jpcc.8b01299>.
- (68) Kopelent, R.; van Bokhoven, J. A.; Szlachetko, J.; Edebeli, J.; Paun, C.; Nachtegaal, M.; Safonova, O. V. Catalytically Active and Spectator Ce³⁺ in Ceria-Supported Metal Catalysts. *Angewandte Chemie* **2015**, *127* (30), 8852–8855. <https://doi.org/10.1002/ange.201503022>.
- (69) Frenkel, A. I.; Yevick, A.; Cooper, C.; Vasic, R. Modeling the Structure and Composition of Nanoparticles by Extended X-Ray Absorption Fine-Structure Spectroscopy. *Annual Review of Analytical Chemistry* **2011**, *4* (1), 23–39. <https://doi.org/10.1146/annurev-anchem-061010-113906>.
- (70) Lykhach, Y.; Staudt, T.; Streber, R.; Lorenz, M. P. A.; Bayer, A.; Steinrück, H.-P.; Libuda, J. CO₂ Activation on Single Crystal Based Ceria and Magnesia/Ceria Model Catalysts. *Eur. Phys. J. B* **2010**, *75* (1), 89–100. <https://doi.org/10.1140/epjb/e2010-00110-x>.
- (71) Li, Z.; Werner, K.; Chen, L.; Jia, A.; Qian, K.; Zhong, J.-Q.; You, R.; Wu, L.; Zhang, L.; Pan, H.; Wu, X.-P.; Gong, X.-Q.; Shaikhutdinov, S.; Huang, W.; Freund, H.-J. Interaction of Hydrogen with Ceria: Hydroxylation, Reduction, and Hydride Formation on the Surface and in the Bulk. *Chemistry – A European Journal* **2021**, *27* (16), 5268–5276. <https://doi.org/10.1002/chem.202005374>.
- (72) Flege, J. I.; Kaemena, B.; Höcker, J.; Bertram, F.; Wollschläger, J.; Schmidt, T.; Falta, J. Ultrathin, Epitaxial Cerium Dioxide on Silicon. *Appl. Phys. Lett.* **2014**, *104* (13), 131604. <https://doi.org/10.1063/1.4870585>.

- (73) Yang, Y.; Mei, D.; Peden, C. H. F.; Campbell, C. T.; Mims, C. A. Surface-Bound Intermediates in Low-Temperature Methanol Synthesis on Copper: Participants and Spectators. *ACS Catal.* **2015**, *5* (12), 7328–7337. <https://doi.org/10.1021/acscatal.5b02060>.
- (74) Kattel, S.; Yan, B.; Yang, Y.; Chen, J. G.; Liu, P. Optimizing Binding Energies of Key Intermediates for CO₂ Hydrogenation to Methanol over Oxide-Supported Copper. *J. Am. Chem. Soc.* **2016**, *138* (38), 12440–12450. <https://doi.org/10.1021/jacs.6b05791>.
- (75) Karelavic, A.; Galdames, G.; Medina, J. C.; Yévenes, C.; Barra, Y.; Jiménez, R. Mechanism and Structure Sensitivity of Methanol Synthesis from CO₂ over SiO₂-Supported Cu Nanoparticles. *Journal of Catalysis* **2019**, *369*, 415–426. <https://doi.org/10.1016/j.jcat.2018.11.012>.
- (76) Senanayake, S. D.; Ramírez, P. J.; Waluyo, I.; Kundu, S.; Mudiyansele, K.; Liu, Z.; Liu, Z.; Axnanda, S.; Stacchiola, D. J.; Evans, J.; Rodriguez, J. A. Hydrogenation of CO₂ to Methanol on CeO_x/Cu(111) and ZnO/Cu(111) Catalysts: Role of the Metal–Oxide Interface and Importance of Ce³⁺ Sites. *J. Phys. Chem. C* **2016**, *120* (3), 1778–1784. <https://doi.org/10.1021/acs.jpcc.5b12012>.
- (77) Li, C.; Sakata, Y.; Arai, T.; Domen, K.; Maruya, K.; Onishi, T. Carbon Monoxide and Carbon Dioxide Adsorption on Cerium Oxide Studied by Fourier-Transform Infrared Spectroscopy. Part 1.—Formation of Carbonate Species on Dehydroxylated CeO₂, at Room Temperature. *J. Chem. Soc., Faraday Trans. 1* **1989**, *85* (4), 929–943. <https://doi.org/10.1039/F19898500929>.
- (78) Li, C.; Sakata, Y.; Arai, T.; Domen, K.; Maruya, K.; Onishi, T. Adsorption of Carbon Monoxide and Carbon Dioxide on Cerium Oxide Studied by Fourier-Transform Infrared Spectroscopy. Part 2.—Formation of Formate Species on Partially Reduced CeO₂ at Room Temperature. *J. Chem. Soc., Faraday Trans. 1* **1989**, *85* (6), 1451–1461. <https://doi.org/10.1039/F19898501451>.
- (79) Appel, L. G.; Eon, J. G.; Schmal, M. The CO₂–CeO₂ Interaction and Its Role in the CeO₂ Reactivity. *Catalysis Letters* **1998**, *56* (4), 199–202. <https://doi.org/10.1023/A:1019098121432>.